HIGH-GAIN MILLIMETER-WAVE ANTENNA DESIGN AND FABRICATION USING MULTILAYER INKJET PRINTING PROCESSES

A Thesis
Presented to
The Academic Faculty

by

Bijan K. Tehrani

In Partial Fulfillment
of the Requirements for the Degree
Master of Science in the
School of Electrical and Computer Engineering

Georgia Institute of Technology
May 2015

HIGH-GAIN MILLIMETER-WAVE ANTENNA DESIGN AND FABRICATION USING MULTILAYER INKJET PRINTING PROCESSES

Approved by:

Professor Manos Tentzeris, Advisor
School of Electrical and Computer Engineering
Georgia Institute of Technology

Professor Gregory Durgin
School of Electrical and Computer Engineering
Georgia Institute of Technology

Professor Andrew Peterson
School of Electrical and Computer Engineering
Georgia Institute of Technology

Date Approved: 23 April 2015

To my father, mother, and sister

ACKNOWLEDGEMENTS

I would first like to thank my advisor Dr. Tentzeris for his continued support and guidance with my research. His encouragement has enabled me to learn and do more than I ever thought I would in my graduate studies while giving me the most wonderful opportunities for my future. I would also like to thank my committee members, Dr. Durgin and Dr. Peterson, for being excellent professors and providing me with insightful feedback on this work.

My sincerest gratitude goes out to my fellow ATHENA lab members: Ben, James, and Sangkil for bringing me in and teaching me how to be a good researcher, as well as John, Jimmy, Jo, Su, and Tao for all of their help and inspiration, creating the best research environment anyone could ask for.

Finally, and most importantly, I would like to thank all of my friends and family for bringing out the best in me. None of this would have been possible without their unending love and support.

TABLE OF CONTENTS

LIST OF TABLES

LIST OF FIGURES

SUMMARY

The research provided in this thesis focuses on the development of high-gain multi-layer millimeter-wave (mm-Wave) antenna structures through additive inkjet printing fabrication processes. This work outlines the printing processes of thick dielectric films for use as printed radio frequency (RF) substrates and provides a proof-of-concept demonstration of the first fully-printed RF structures. Using the outlined processes, demonstrations of high-gain mm-Wave proximity-coupled patch array and Yagi-Uda array antennas are presented, achieving the highest realized gain within the 24.5 GHz ISM band for inkjet-printed antennas in literature.

Chapter 1 introduces the concept of inkjet printing and its interest for integration with mm-Wave wireless technology, as well as related previous efforts.

Chapter 2 outlines the standard processes used within inkjet printing as well as popular metallic conducting and insulating dielectric ink materials.

Chapter 3 introduces several advanced inkjet-printing processing techniques geared towards the realization of thick, uniform dielectric films, presenting the demonstration of the first fully-printed RF structures as a proof-of-concept.

The work presented in Section 3.2 is published in *2014 IEEE MTT-S International Microwave Symposium (IMS) Proceedings* and is reference [29] in this thesis.

Chapter 4 presents the design, fabrication, and measurement of high-gain mm-Wave proximity-coupled patch array and Yagi-Uda array antennas, achieving the highest realized gain within the 24.5 GHz ISM band for inkjet-printed antennas in literature.

The work presented in Section 4.1 is published in *IEEE Antennas and Wireless*

Propagation Letters and is reference [8] in this thesis.

The work presented in Section 4.2 is under review for publishing in *IEEE Antennas and Wireless Propagation Letters* and is reference [30] in this thesis.

Finally, Chapter 5 summarizes the contributions of the work within this thesis and discusses potential paths of research for the future.

CHAPTER I

INTRODUCTION

In the field of electronic device manufacturing and packaging, inkjet printing is a fabrication technology that has been gaining attention throughout the past decade as a method to rapidly realize low-cost passive and active devices, such as lumped components, planar antennas, and various semiconducting devices. Inkjet printing has the advantage of additively depositing a variety materials in the forms of inks with conductive, dielectric, and nanomaterial compositions [5,7,16,26]. This patterning process removes a majority of the dependence upon the host substrate that is typically present in traditional fabrication methods, allowing for a virtually infinite catalog of electronic substrates, ranging from flexible, low-temperature organics to rigid semiconductors and glasses.

Until recently, inkjet printing has been used to fabricate planar, single-layer antennas for radio-frequency identification (RFID) and ultra-wideband (UWB) communication, reaching up to 10 GHz in operation [21,31]. With the increasing congestion of the popular RFID and sub-10 GHz frequency bands, the current advancement of wireless technology is pushing for higher frequencies of operation [17]. Such applications of automotive radar and gigabit wireless communication have brought interest to the millimeter-wave (mm-Wave) frequency spectrum, extending from tens of GHz up to the sub-THz range. This higher operational frequency introduces wider bandwidths for communication purposes, which is useful for sensitive Doppler radar, wireless imaging, and high data rate transmission.

Conventional mm-Wave antenna fabrication includes the subtractive patterning of metals on a multilayer laminate substrate or wafer [11, 23]. These subtractive

methods, including lithographic etching and mechanical milling, are based on the removal of metallic and dielectric material from a host material to pattern the desired antenna structure. The removal of these materials produces chemical and material waste while requiring a relatively high cost and fabrication processing time, which could be avoided through the use of additive fabrication methods.

In recent work, inkjet printing has been demonstrated as a useful method of fabrication for mm-wave antenna structures operating within 24.5 and 60 GHz ISM bands. Wideband Vivaldi and series-fed two-dipole antennas have been inkjet-printed directly on flexible liquid crystalline polymer (LCP) substrates, demonstrating operation throughout the 24.5 GHz ISM band and up to 40 GHz [20, 27]. Coplanar waveguide-fed (CPW) monopole antennas have been demonstrated with inkjet printing on flexible polyethylene-based substrates for 60 GHz applications [1, 12]. These designs have varying degrees of efficiency and potential for a variety of applications, however they suffer from several limitations present in typical multilayer RF structure design. Inkjet printing is used to fabricate these planar antenna topologies onto common laminate substrates that have limitations of discrete thicknesses and material properties. In order to fabricate multilayer antenna structures, multilayer laminate substrate processing techniques must be utilized, including material stacking, bonding, and alignment. Each of these factors introduce their own degrees of error to the final structure of the multilayer antenna.

With the utilization of the selective deposition of thick dielectric inks in conjunction with metallic conducting inks through inkjet printing, multilayer structures have the potential to be fabricated directly onto host substrates, eliminating the need for multilayer laminate processing. Significant research has been performed as a background to these methods to allow for the integration of multilayer structures with inkjet printing processes. Benjamin S. Cook (Georgia Institute of Technology) has outlined and demonstrated a multilayer printing process for the realization

of multilayer, vertically-integrated RF passive components, antennas, and microfluidic platforms [4]. Additionally, Sangkil Kim (Georgia Institute of Technology) has demonstrated the integration of inkjet printing with susbtrate integrated waveguide (SIW) technology through the realization of inkjet-printed flexible via structures [15]. Through the continued development and refinement of these methods, multilayer mm-Wave antenna structures can be realized in a low-cost, rapid process for the potential post-process integration with on-chip/on-package systems and flexible organic substrates. In order for this method of fabrication to functionally compete with conventional laminate-based stack-ups, inkjet printing must utilize well characterized ink materials and processing techniques.

1.1 Research Objectives

The objective of this thesis is to demonstrate the feasibility of realizing multilayer, high-gain antennas in the millimeter-wave range through the additive fabrication process of inkjet printing. Specifically this work focuses on the following points:

1. The formulation and characterization of nanoparticle-based conductive and polymer-based thick-film dielectric inks and processing techniques

2. The design, fabrication, and measurement of high-gain multilayer antennas operating within the 24.5 GHz ISM band utilizing the selective additive deposition of metallic and thick dielectric materials

1.2 Thesis Outline

This thesis is outlined as follows:

- Chapter 2 outlines the standard processes used within inkjet printing as well as popular metallic conducting and insulating dielectric ink materials.

- Chapter 3 introduces several advanced inkjet-printing processing techniques geared towards the realization of thick, uniform dielectric films and presents the demonstration of fully-printed multilayer RF structures as a proof-of-concept.

- Chapter 4 outlines the design, fabrication process flow, and measurements of proximity-coupled patch and Yagi-Uda antenna arrays operating within the 24.5 GHz ISM band.

- Chapter 5 concludes the results of this research and discusses future advancements and applications.

CHAPTER II

INKJET PRINTING MATERIALS AND PROCESSES

Inkjet-printed electronic systems require a catalog of printable ink formulations, including conductive and dielectric materials. These inks can have a variety of material compositions, including metal catalyst, nanoparticle, and polymer bases. Aside from ink materials, the fundamental success of inkjet printing lies within the reliable agreement between printed inks and host substrates, which must be assessed in order to achieve efficient and repeatable electronic fabrication.

2.1 Processing Techniques

In order for a micron-sized pattern to be deposited onto a substrate using inkjet printing, several material factors must be considered, including ink jetting characteristics and substrate surface characteristics.

2.1.1 Ink Temperature and Jetting Voltage

The effectiveness of an inkjet-printed fabrication begins with ink jetting characteristics. Using a piezoelectric droplet jetting system, the voltage of the piezoelectric actuator helps determine the formulation and expulsion of ink droplets from the cartridge. In operation, a time dependent voltage waveform is utilized to bring the actuator through stages of intake, drop jetting, and recovery. Figure 1 shows a generalized cartridge waveform for ink jetting. The voltages required to expel well-formed droplets from the cartridge relate heavily to the viscosity and temperature of the ink, which are typically in the order of 12–15 cP and 30–40 °C, respectively [7].

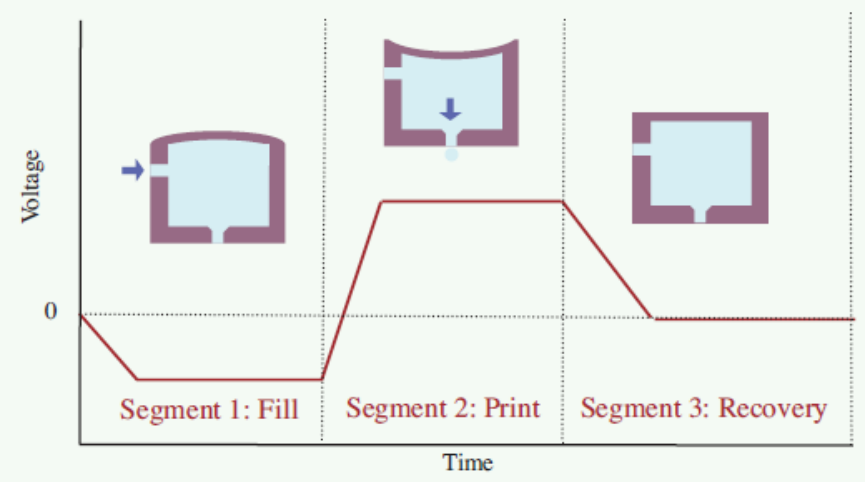

Figure 1: General acuator waveform for ink jetting [25].

2.1.2 Substrate Surface Energy Modification

Once a droplet is expelled from the cartridge, material agreement between the ink and the substrate must be made in order to produce an accurate, repeatable pattern. This agreement is made with the relationship between the surface energy of the substrate and the surface tension and contact angle of the ink. When the surface energy of the substrate is much higher than the surface tension of the ink droplet, the contact angle of the ink will be too small and the ink will spread greatly from its initial drop diameter. In the inverse situation, the contact angle of the ink droplet will be too high and will pull away from the substrate [19]. Typically, good wetting of an ink to a substrate occurs when the surface energy of the substrate is greater than the surface tension of the ink by 10–20 mN/m. The surface energy of a substrate can be modified through raising the temperature of the substrate or UV ozone surface treatment, which will decrease and increase the surface energy of the substrate, respectively.

Figure 2 shows a general contact angle measurement of a liquid droplet on a solid substrate that is used to determine the surface energy of a substrate. The variables γ_{sv}, γ_{sl}, and γ_{lv} represent the free energies between solid/vapor, solid/liquid, and liquid/vapor interfaces, respectively [19]. The relationship of these energies with

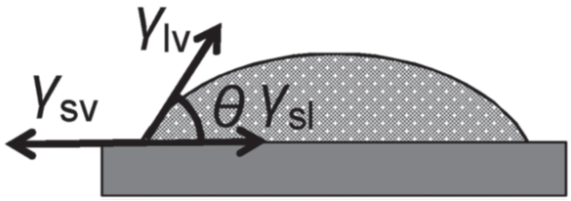

Figure 2: Droplet wetting on substrate displaying contact angle θ, used to determine substrate surface energy [19].

a contact angle can be simplified and expressed with planar geometry as Young's relation, shown in Equation 1 [3]:

$$\gamma_{sv} = \gamma_{sl} + \gamma_{lv} \cos\theta \tag{1}$$

2.2 Ink Formulation and Characterization

As previously stated, reliable inkjet printing requires fine-tuned ink formulations consisting of a certain viscosity and surface energy. Multilayer inkjet-printed devices require the use of both high conductivity metallic inks and thick film dielectric inks in order to allow for structural versatility, device miniaturization, and purely selective system deposition.

2.2.1 Silver Nanoparticle-Based Ink

One of the most popular options for inkjet-printed conductive materials is a silver nanoparticle-based solution, specifically the CCI-300 ink formulation provided by Cabot (Cabot Corporation, Boston, MA, USA). These solutions are composed of a dispersion of 30–50 nm diameter silver nanoparticles in an organic solvent solution, usually ethanol and ethanediol. Once deposited, curing must take place in order to remove the solvent from the ink. Do to the nature of the solvent, the solvent is able to evaporate at a relatively low temperature of 60 °C. Once the solvent is evaporated, the volume of metallic nanoparticles are sintered using an oven from 120-200 °C for up to 2 hours to allow for the evaporation of particle coatings and particle necking.

One alternative method of sintering is through the use of a rastering laser, which can bring down sintering time to minutes [7]. These methods of deposition and curing have demonstrated conductivity in the order of 10^7 S/m, 5x less than that of bulk silver, with a layer thickness of approximately 500 nm per layer.

Another silver nanoparticle-based ink option is Silverjet DGP-40LT-15C provided by ANP (ANP Corporation, Sejong-si, South Korea). This solution contains 30–35 w% silver nanoparticles dispersed within a triethylene glycol monoethyl ether (TGME) solvent, exhibiting a viscosity of 10 cP and a surface tension of 35 mN/m. Once printed, the metallic ink follows a processing flow similar to that of the Cabot CCI-300 ink, yielding 800 nm thick layers with a resistivity of 11 $\mu\Omega$-cm [29].

2.2.2 Thick Film Polymer-Based Ink

Commonly used as a photoresist in integrated circuit (IC) fabrication, SU-8 is a long-chain polymer that is deposited through spin-coating onto silicon wafers for electronic device patterning. Recent advances in inkjet printing have allowed for this polymer to go beyond its typical cleanroom use as a sacrificial mask towards a thick film dielectric for microwave devices [5, 6, 29]. SU-8 polymer chains have two advantages for inkjet printing fabrication: low-temperature UV cross-linking and high polymer content by weight while still maintaining a relatively low viscosity [14]. Low-temperature processing is useful when dealing with organic substrates typically used with inkjet printing that may deteriorate at higher temperatures, such as paper and LCP. High polymer content allows for a thicker, more uniform layer-by-layer deposition, while low viscosity is required to be compatible with industrial inkjet printer cartridges. In order to ensure viscous compatibility, SU-8 ink is formulated with the addition of a cyclopentanone solvent. Once deposited, standard cleanroom baking and cross-linking procedures are performed to finalize the patterned dielectric film.

The microwave properties of the SU-8 polymer are advantageous for use as a thick

dielectric film, with a relative permittivity of approximately 2.85 and a loss tangent of 0.004 up to 40 GHz [8]. SU-8 films can be deposited with a thickness of 4-6 μm per layer using a 20 μm drop spacing, shown in Figure 3. The nonuniformity in the profile of printed SU-8 thick films is known as the "coffee ring effect" and is the result of surface tension mismatches between the deposited ink and the host substrate as well as material drying profiles [19]. Special surface treatment and variable baking temperatures are commonly used to minimize issues with SU-8 film uniformity and allow for the fabrication of uniform printed dielectrics exceeding 100 μm in thickness.

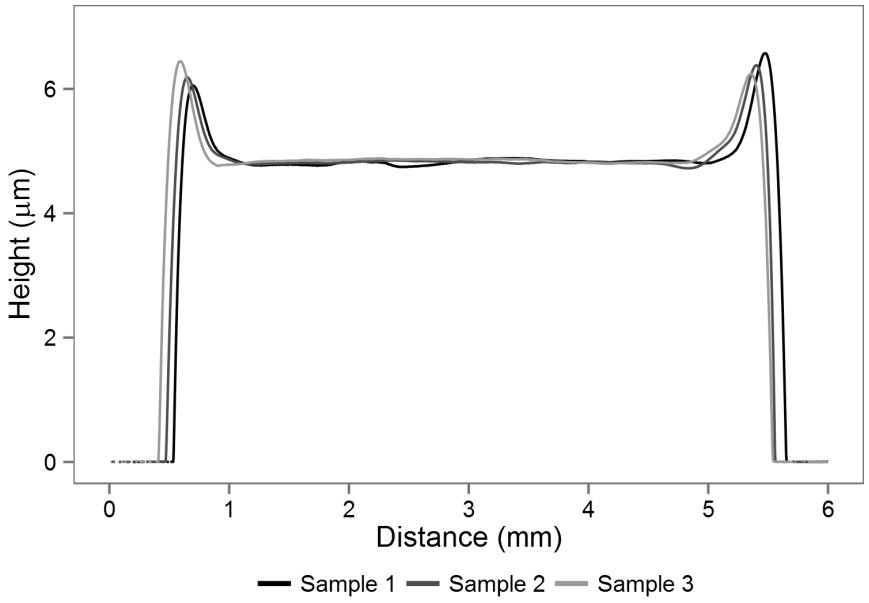

Figure 3: Profilometer measurements of printed single-layer SU-8 films.

CHAPTER III

INKJET PRINTING THICK DIELECTRIC FILMS

In order to establish a robust printing scheme for multilayer antenna structures, several processing techniques must be employed for use with thick film polymer-based inks. A dielectric structure used for this purpose must be able to be deposited in an efficient, uniform manor in order to ensure both predictability with modeling and reliability with fabrication. These goals can be achieved through the utilization of several advanced processing techniques discussed within this chapter. As a demonstration, fully-printed RF structures are also presented, where all multilayer components (ground, dielectric substrate, vias, and microstrip topology) are realized through additive inkjet printing manufacturing.

3.1 Advanced Thick Film Ink Processing Techniques

As previously discussed, there are several issues present in the surface profiles of printed dielectric films that result from surface energy mismatches and material drying profiles. These issues have the potential to multiply with the printing of multiple layers, yielding thick dielectric substrates without uniform profiles, essentially reducing practicality for antenna structure fabrication. Profilometer scans of printed multilayer SU-8 dielectric films are shown in Figure 4 for 1-, 3-, 5-, 7-, and 9-layer prints. As the number of printed layers increases, the "coffee ring" profile tendencies present in single-layer prints merge into larger-scale profile uniformity issues, where variation in the range of 20% of total printed thickness can be witnessed, for example with the 7-layer print in Figure 4. In order to assess this issue and improve profile uniformity throughout a printed film while ensuring multilayer printing capabilities, several advanced processing techniques can be employed: UV ozone surface

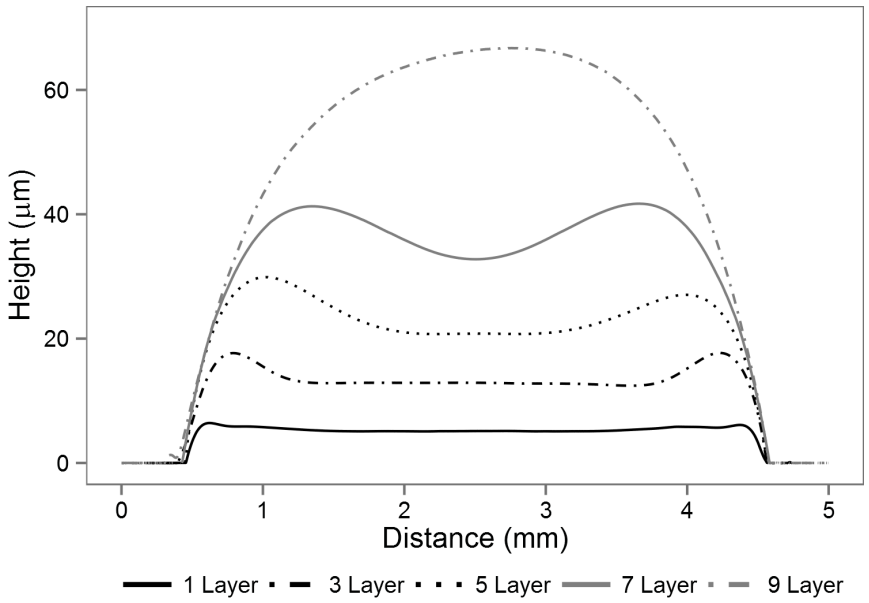

Figure 4: Profilometer measurements of printed multilayer SU-8 films.

modification, thermal reflow, and multi-session printing.

3.1.1 UV Ozone Surface Modification

The wetting of an ink droplet, no matter its chemical composition, is subject to the surface tension of the ink material and surface energy of the host substrate. As previously discussed, mismatches in these properties can result in ink droplets spreading or "balling-up" upon interaction with a substrate, often defining the integrity of a printed pattern. In order to tune this crucial interaction, the surface energy of a substrate can be modified and tuned with the use of UV ozone exposure. This process is especially important in the desired utilization of inkjet-printed dielectric films as multilayer RF antenna substrates.

In order to understand the interaction of ink materials with printed dielectric films, contact angle and surface energy measurements are performed on a printed SU-8 dielectric film. Figure 5 shows a parametric exposure of a printed SU-8 film with UV ozone exposures up to 210 seconds using a UVO Cleaner Model No. 42 provided by Jelight (Jelight Company Inc., Irvine, CA, USA). As exposure time

increases, the surface energy of the printed SU-8 film approaches a saturation energy around 45 mN/m. This process demonstrates the tunability of the surface energy of a printed-film in order to ensure proper wetting with other inkjet printing materials, such as metallic inks, in order to realize multilayer printed structures.

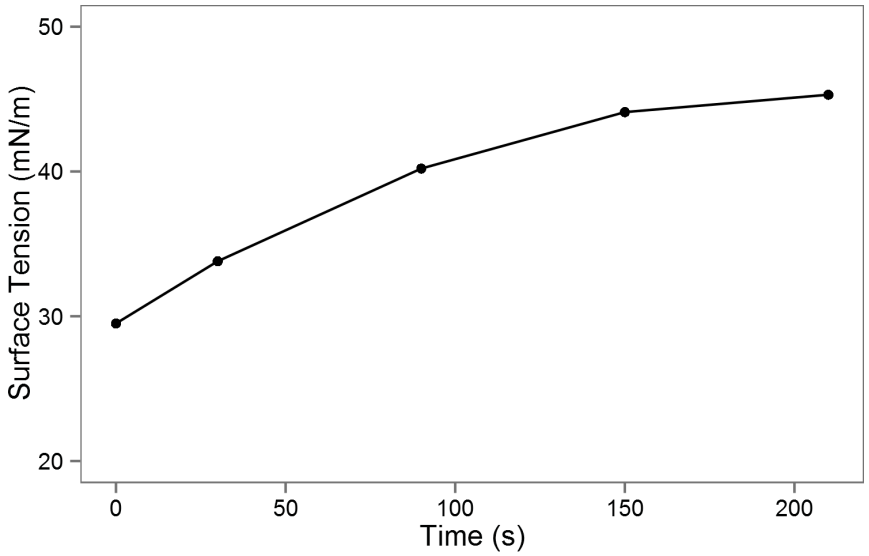

Figure 5: Surface energy measurements for printed SU-8 dielectric films with various durations of UV ozone exposure.

3.1.2 Thermal Reflow

The surface uniformity of printed dielectric films is very important in the realization of multilayer printed structures. When multiple stacked topologies are desired, theses variations in uniformity have the potential to add and multiply of the process of the fabrication and cause great issue for overall system reliability. For this reason, it is desired to improve the profile uniformity of inkjet-printed films. This can be achieved through the use of a thermal reflow treatment on a printed polymeric film. The process begins directly after printing during the initial soft bake, where temperature is raised beyond the typical processing temperature to 150 °C. By increasing the temperature, the viscosity of the pre-cured film decreases, causing the profile to deform and the heightened edges of the film to settle into a more uniform shape.

Figure 6 shows the result of a thermal reflow process on a printed SU-8 dielectric film for different durations of time. Both the initial shape of the film and the time of reflow are important parameters that must be considered when performing reflow processing. As is shown with the 5 and 10 min processing durations in Figure 6, excessive thermal processing can lead to over-deformation and a convex, nonuniform resulting profile. Once the desired profile is achieved during the thermal processing of the soft bake, standard curing processes are applied to finalize the patterning of the uniform dielectric film.

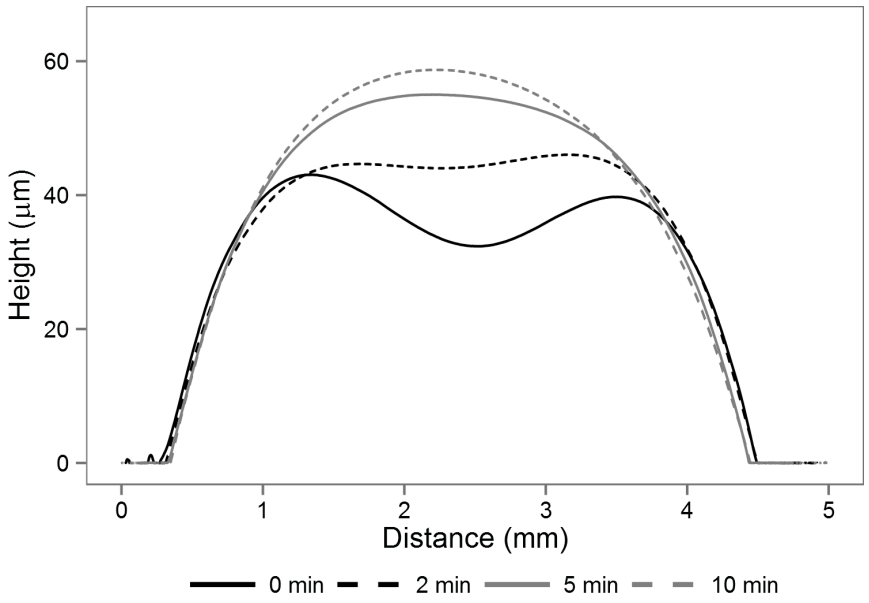

Figure 6: Profilometer measurements of printed SU-8 dielectric films with various durations of 150 °C thermal reflow processing.

3.1.3 Muli-Session Printing

As previously discussed, the profile of an inkjet-printed dielectric film depends on several factors, including the area of the structure and the number or printed layers. When many layers of material are printed within a single area, profile deformities can arise, such as the 9-layer print shown in Figure 4. The large amount of material deposited within a certain area causes the film to bulge and create a convex drop-like structure. In order to avoid this nonuniform structure, multi-session printing can be

utilized.

Multi-session printing involves the use of multiple printing and curing sessions to realize thick, uniform dielectric structures without issues of material bulging. The process begins with an analysis of printed layer count and resulting film profile. Once a desired profile is achieved, typically involving the maximum amount of printed layers before a convex profile is formed, the printing session is repeated in order to yield the desired dielectric film thickness. Figure 7 shows profilometer scans of printed SU-8 dielectric profiles with multisession 7-layer prints [28]. Through the use of multi-session printing, uniform dielectric structures exceeding 100 μm are able to be realized with inkjet printing technologies for the selective patterning of thick dielectric substrates.

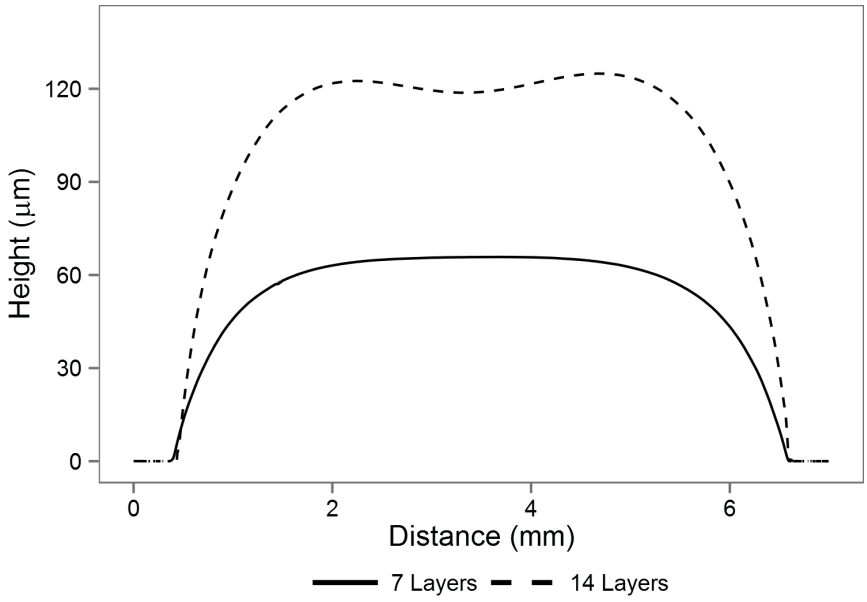

Figure 7: Profilometer measurements of printed SU-8 dielectric films with 7-layer and 7-layer + 7-layer (14 layers total) multi-sessions printing.

3.2 Fully-Printed RF Structures with Dielectric Substrates

In order to demonstrate the utility of inkjet-printed thick dielectric films, fully-printed vias, RF microstrip lines, and T-resonator structures are fabricated to characterize

the SU-8 dielectric ink [29]. These structures are used demonstrate multilayer printed interconnects and extract the loss and relative permittivity of the printed SU-8 material from 0–30 GHz. The realization of thick dielectric substrates and vias with inkjet printing helps advance the development of fully-printed multilayer and substrate-independent antenna structures, further distancing design and fabrication from bulk laminate substrate restrictions.

3.2.1 Multilayer Vias

From an additive approach, vias are constructed through a lack of material deposition in a small area. One issue with this additive approach of via fabrication is the presence of slanted walls on the edges of printed dielectric structures. Multi-session printing of dielectric layers increases the slope of the walls of dielectric structures, shown in Figure 8(a), helping to conform the shape of inkjet-printed vias to traditional vertical-wall vias. The ramp-up distance of the SU-8 sidewalls from zero thickness to the nominal dielectric thickness is found to be approximately 1 mm.

A test structure is fabricated in order to determine the DC resistance of the inkjet-printed vias. A 4-layer (25 μm) SU-8 dielectric structure with via holes is printed on top of ten traces of 4-layer (3 μm) Silverjet DGP-40LT-15C silver nanoparticle ink. Finally, 4-layer silver traces are printed on top of the dielectric substrate with and without the via connection to the bottom traces in order to determine the DC resistance of the ramp-up vias. A micrograph of an inkjet-printed via is shown in Figure 8(b). Comparing the DC resistances of the complete and incomplete traces, the printed samples yield an average DC resistance of 0.073 Ω with a standard deviation of 0.041 Ω for the 1 mm length ramp-up vias, which is an improvement on the efficiency [13, 22] and variance [9] of inkjet-printed vias presented in previous works. Table 1 provides a summary of the printed via DC resistance measurements.

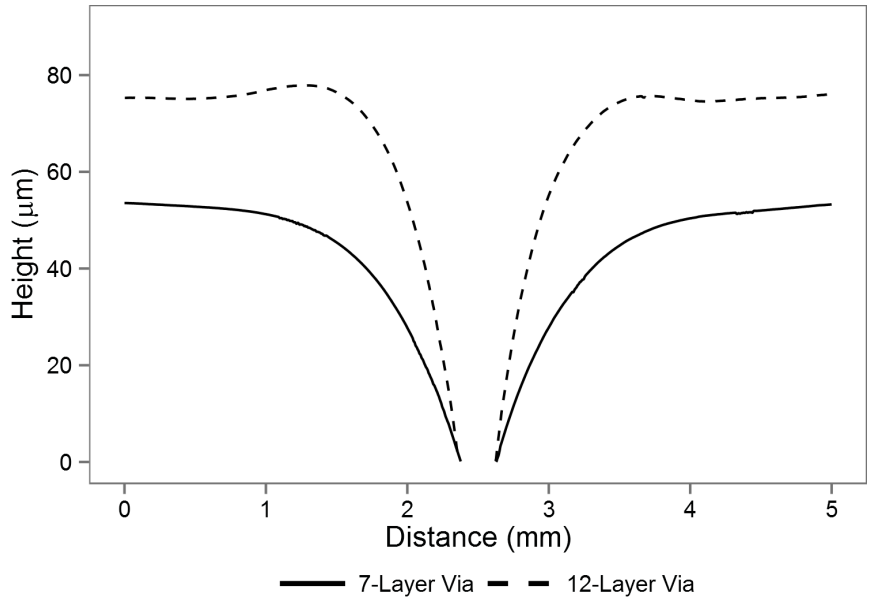

(a)

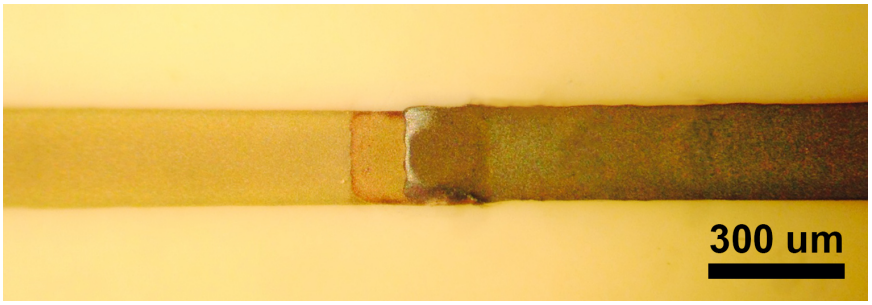

(b)

Figure 8: (a) Profilometer scans of inkjet-printed vias realized in 7- and 12-layer SU-8 dielectric substrates. (b) Micrograph of printed via transition test structure fabricated to measure DC resistance of ramp-up vias.

Table 1: Summary of Measured DC Resistances of Inkjet-Printed Vias

	Incomplete Lines (Ω)		**Completed Lines (Ω)**
	Top	Bottom	
	0.345	0.251	0.692
	0.328	0.267	0.617
	0.345	0.238	0.623
	0.310	0.241	0.693
	0.298	0.250	0.631
	0.361	0.251	0.685
	0.354	0.235	0.654
	0.364	0.252	0.606
	0.342	0.247	0.676
	0.286	0.238	0.660
Average	0.333	0.247	0.654
Std. Dev.	0.026	0.009	0.031
Via Average	0.073		
Via Std. Dev.	0.041		

3.2.2 Microstrip Line

To demonstrate the concept of using SU-8 dielectric ink as a thick RF substrate, a microstrip line is fabricated on a printed SU-8 film with Silverjet DGP-40LT-15C silver nanoparticle ink. In order to allow for ground-signal-ground (GSG) probe feeding and measurements, a CPW-to-microstrip line transition is included in the design. The thickness of the SU-8 substrate is chosen to be 80 μm to yield a feasible microstrip line width and CPW gap (100 μm spacing between signal and ground). The CPW-to-microstrip line transition is printed near the edge of the SU-8 substrate, where the CPW ground lines are extended down to the ground plane of the circuit. Images of the microstrip line with CPW-to-microstrip line transitions are shown in Figure 9.

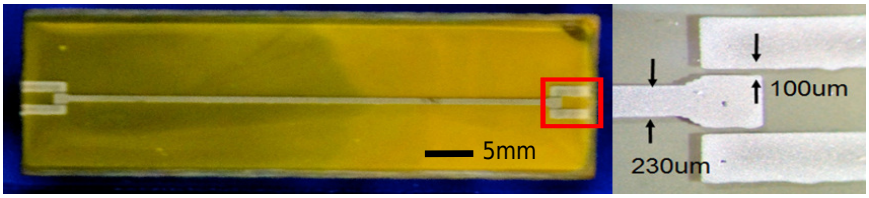

Figure 9: Micrographs of fully-printed microstrip line with CPW to microstrip line transition.

In order to characterize the line loss and group delay of the microstrip line, a 37369A vector network analyzer (VNA) provided by Anritsu is utilized (Anritsu Company, Kanagawa, Japan). The effects of the probes and feed lines are de-embedded with the use of a printed TRL calibration kit following the same processing conditions. The line loss and group delay of the 6 mm microstrip line with respect to frequency are shown in Figure 10(a) and 10(b), respectively, from 1–30 GHz. The line loss increases as frequency increases because of an increase in dielectric loss and surface resistance. Additionally, radiation from the line also increases with frequency. The group velocity decreases slightly at lower frequencies yet remains fairly constant above 5 GHz up to 30 GHz.

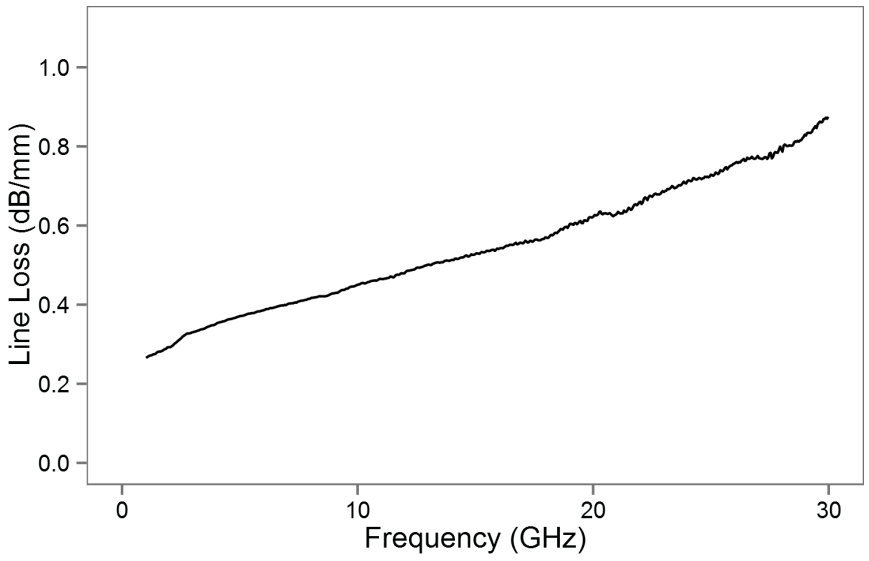

(a)

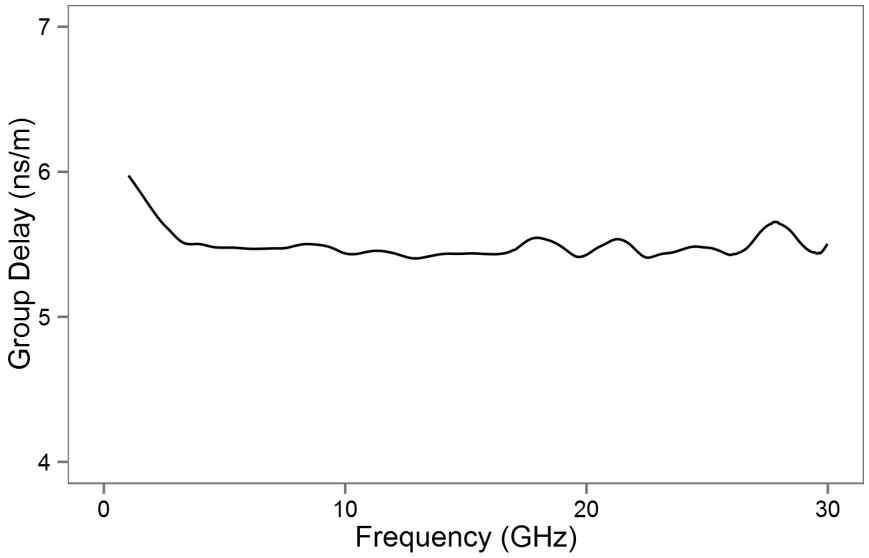

(b)

Figure 10: Measurements of fuly-printed microstrip (a) line loss and (b) group delay as a function of frequency.

3.2.3 T-Resonator

Another structure commonly utilized for RF material characterization is the T-resonator, which can be easily fabricated using the multilayer process previously outline. As a proof-of-concept demonstration, a purely additive microstrip T-resonator

with a fundamental resonant frequency at 2.21 GHz is utilized for the RF characterization of this completely inkjet-printed structure, consisting of a full ground plane, SU-8 dielectric substrate, and microstrip topology. Figure 11 shows the fabricated T-resonator, including a microstrip transmission line with length 19.8 mm and a microstrip resonating line with length 19.5 mm.

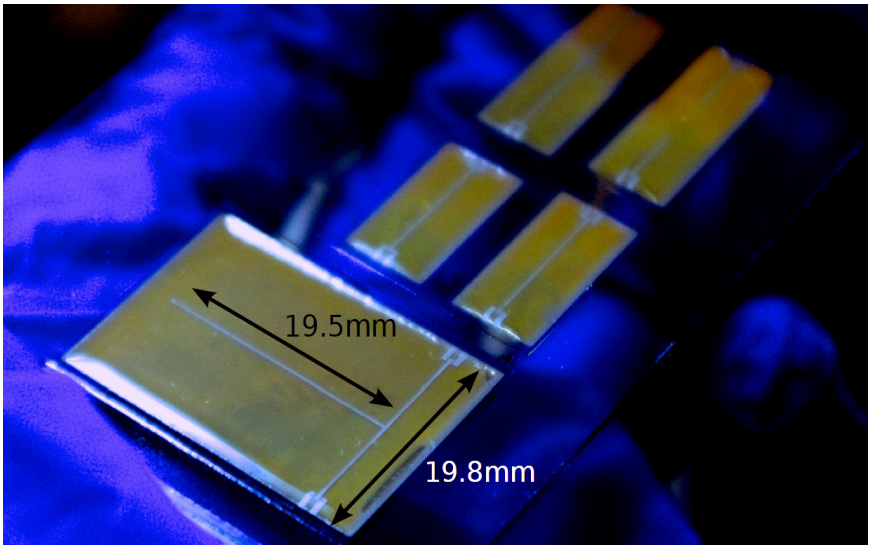

Figure 11: Image of fully-printed T-resonator, microstrip lines, and TRL calibration kit.

Using the harmonics of the resonant frequency at 2.21 GHz, the T-resonator is used to extract the relative permittivity of the SU-8 substrate up to 30 GHz. To validate the accuracy of the characterization, both T-Resonator and two line methods are adopted [2, 18, 32]. The relative permittivity values obtained through the use of these two methods are shown in Figure 12. Both of the results compare well with results gathered in previous works [10]. As frequency increases, measurements also agree with the expected trend in the material characteristics of the SU-8 dielectric, where the relative permittivity gradually decreases.

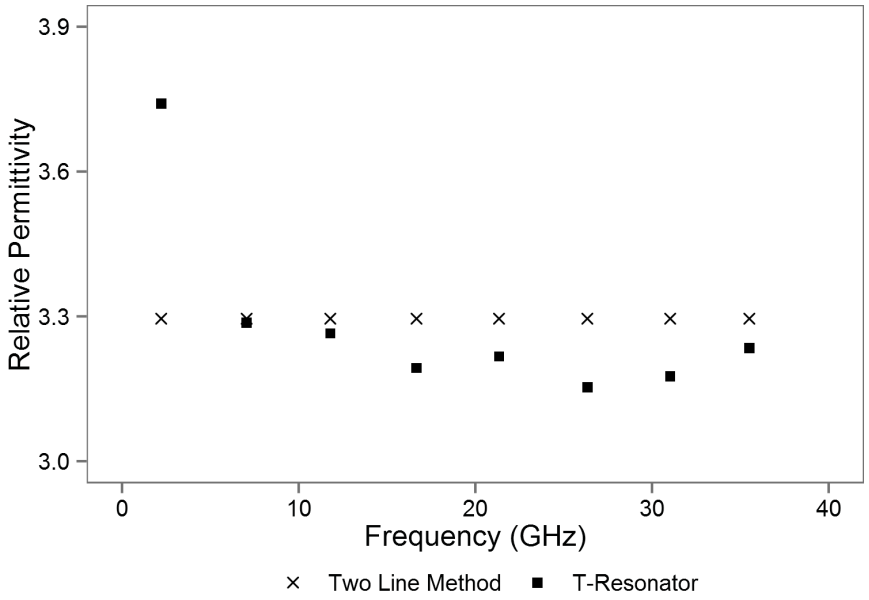

Figure 12: Measurements of relative permittivity for inkjet-printed SU-8 substrate.

CHAPTER IV

MILLIMETER-WAVE ANTENNA DESIGN AND FABRICATION

With conductive and dielectric inks established, inkjet printing can be used to realize multilayer RF structures reaching into the mm-Wave frequency range. The additive nature of this fabrication method allows for the development of multilayer, vertically-integrated antenna structures for use with flexible organic substrates, on-chip post-processing, and the use of novel low-temperature substrates while reducing fabrication time and material waste from traditional methods.

In this chapter, two multilayer inkjet-printed antenna structures are presented for operation within the 24.5 GHz ISM band. The first design is an adaptation of the canonical patch antenna array utilizing proximity-coupled feeding [8]. The second design is a Yagi-Uda antenna array featuring an unbalanced (microstrip) to balanced (slotline) excitation [30].

4.1 Proximity-Coupled Patch Antenna Array

To demonstrate the multilayer inkjet printing process with conductive and thick dielectric inks, a 4-element proximity-coupled patch antenna array is designed for use within the 24.5 GHz ISM band [8]. The proximity-coupled feeding technique improves the matching of the patch to the 50 Ω microstrip feed line while also increasing the bandwidth of operation. The patch arrays are modeled, simulated, and optimized within the CST Microwave Studio Suite, yielding an optimal center-to-center element spacing of 0.51λ in the horizontal direction and 0.6λ in the vertical direction. The dimensions of the patch elements are determined to be 3.5×4.4 mm^2. A model of

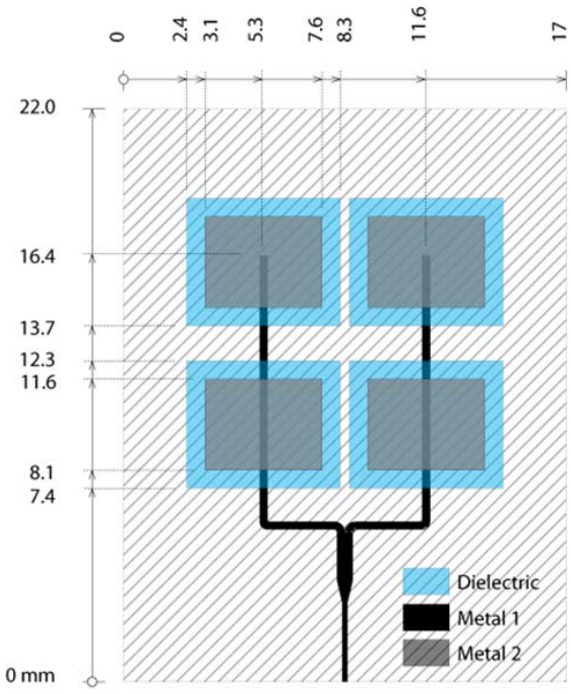

Figure 13: Topological model of 24.5 GHz proximity-coupled patch antenna array.

the patch array is shown in Figure 13.

4.1.1 Fabrication Process Flow

With traditional fabrication techniques, the proximity-couple patch array requires two laminate substrates: a host substrate and a dielectric spacer; along with three metallic patterns: a ground plane, microstrip feed lines, and resonant patches. Utilizing inkjet printing, the substrate is reduced to one material with selectively patterned dielectric spacers, avoiding any laminate bonding or subtractive patterning.

A diagram outlining the processes flow is displayed in Figure 14. Using a Dimatix DMP-2831 inkjet printing system, three layers of Cabot CCI-300 silver nanoparticle ink are printed onto a single-clad Rogers LCP substrate. The printed silver is then cured and sintered with the thermal baking profile outlined in Section 2.2.1 to finalize the microstrip feed lines. After sintering, the substrate is treated with 30 seconds of UV ozone exposure and 10 layers of SU-8 dielectric are printed to achieve the 60 μm spacer thickness. The SU-8 then undergoes a pre-exposure curing at 90 °C for 5

minutes, exposure to 365 nm UV light for cross-linking, and post-exposure curing at 120 °C for 5 minutes. After another UV ozone treatment for 90 seconds, three silver layers are printed to pattern the top patches with curing and sintering profiles similar to the previous metal layer, concluding the fabrication process.

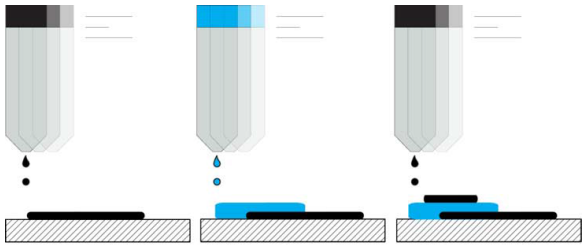

Figure 14: Fabrication process flow for inkjet-printed proximity-coupled patch antenna array showing the printing of silver (black) and SU-8 (blue) inks.

A micrograph image of the printed proximity-coupled patch array is shown in Figure 15. Physical measurements of the printed samples show good agreement with the model topology, with the exception of a dielectric thickness of 64 μm, 4 μm greater than the desired dielectric thickness. The dimensions of the fabricated patch elements are measured to be 3.52 $\times$ 4.5 mm^2, yielding a maximum 2.3% variation from the initial dimensions.

4.1.2 Results and Analysis

Upon completion of fabrication, end-launch 2.92 mm connectors from Southwest Microwave (Southwest Microwave, Tempe, AZ, USA) are mounted to the printed antenna and return loss of the samples is measured using an Anritsu 37369A VNA. Simulated and measured return loss is shown in Figure 16, showing good agreement with both printed samples at 24.75 GHz. The frequency at which the fabricated antennas experience the best matching is approximately 1% higher than the intended frequency due to small fabrication variations, but good matching is achieved through post-fabrication simulation.

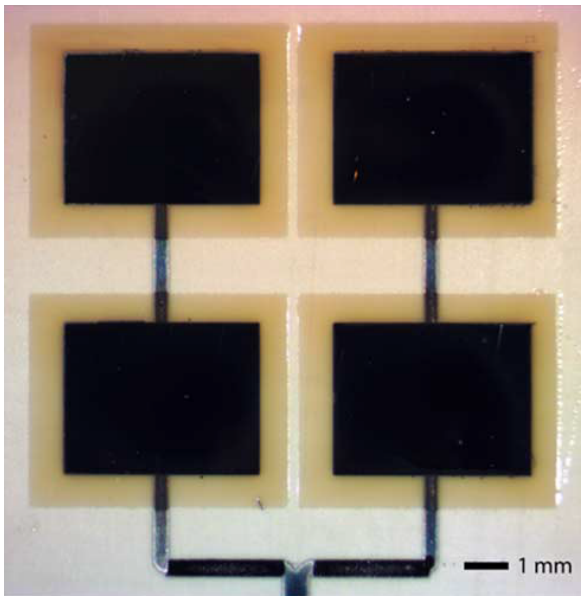

Figure 15: Micrograph of fabricated proximity-coupled patch antenna array.

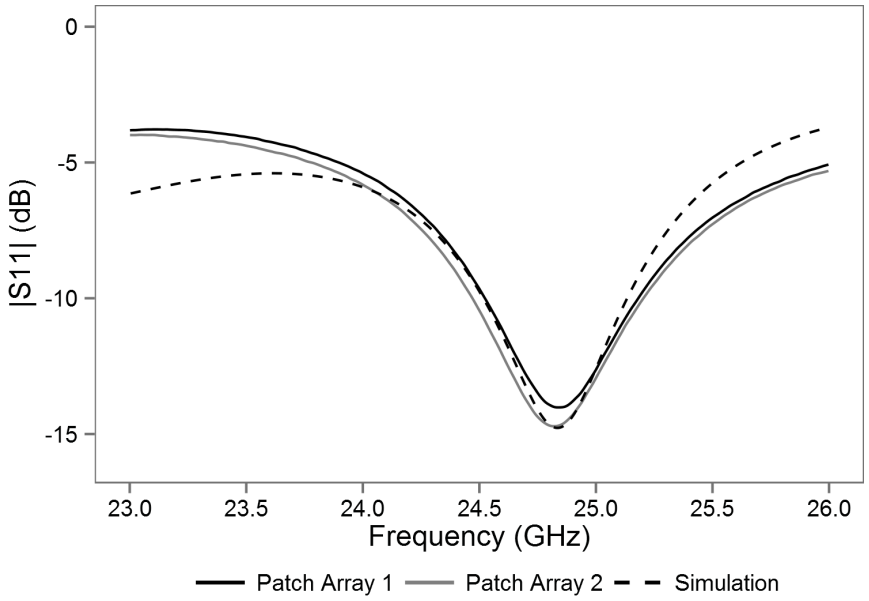

Figure 16: Simulated and measured return loss for printed patch arrays.

The radiation patterns and broadside realized gain of the printed arrays are measured within a far-field anechoic chamber utilizing standardized gain horns. The gain and pattern measurements are shown in Figure 17 and Figure 18, respectively. The measured magnitude of broadside realized gain matches well with the simulation,

reaching up to 7 dBi. Normalized E and H-plane radiation patterns show good agreement with simulations, with exception to the 180° direction due to the presence of the end-launch connector and its exclusion from simulations.

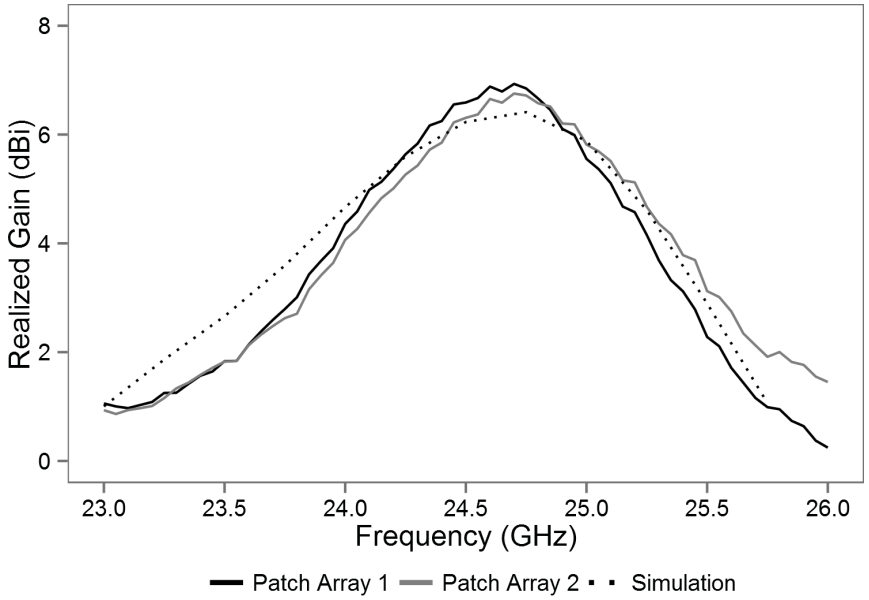

Figure 17: Simulated and measured broadside realized gain versus frequency of the proximity-coupled patch arrays.

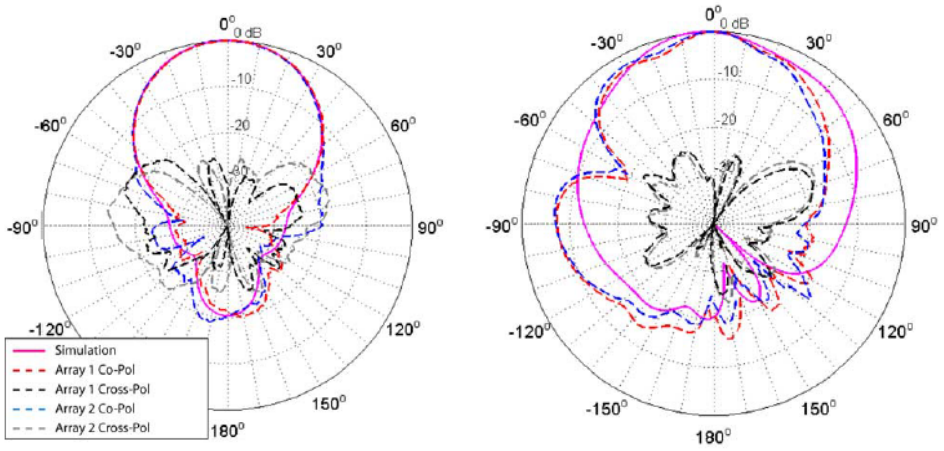

(a) (b)

Figure 18: Simulated and measured normalized (a) H-plane and (b) E-plane radiation patterns.

4.2 Multilayer Yagi-Uda Antenna Array

As another demonstration of multilayer inkjet printing fabrication technology, multi-director Yagi-Uda antenna arrays are designed for the 24.5 GHz ISM band [30]. In order to reach a balance between end-fire gain and antenna size, 3- and 5-director topologies are modeled, simulated, and optimized within the CST Microwave Studio Suite. The design includes a transition from a microstrip feed to a slotline feed for matching and test equipment integration [24]. A model of the 3- and 5-director Yagi-Uda arrays is shown in Figure 19.

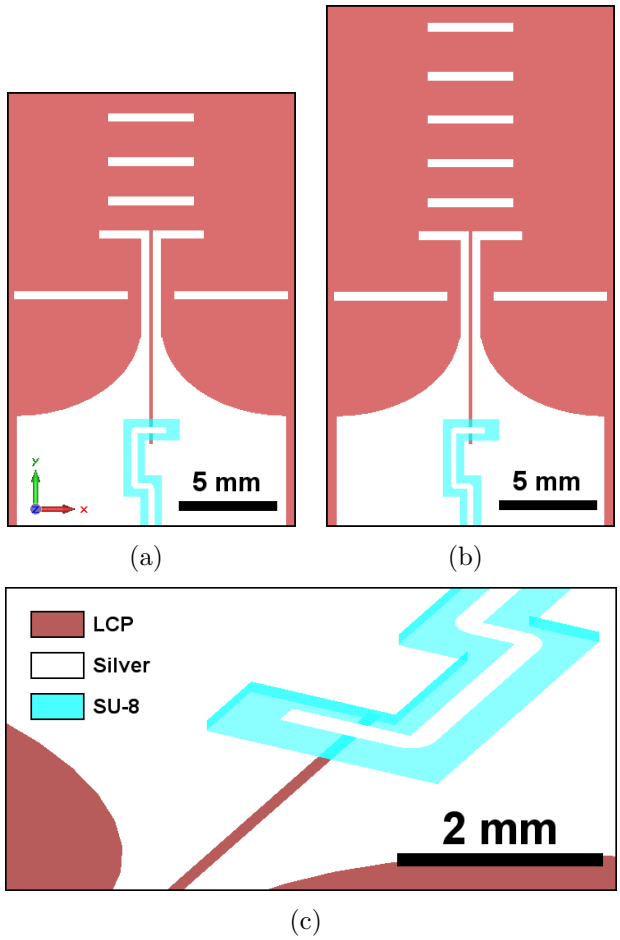

Figure 19: Simulation models for inkjet-printed (a) 3- and (b) 5-director Yagi-Uda antennas with (c) detail showing a multilayer microstrip-to-slotline transition.

4.2.1 Fabrication Process Flow

The process flow for the fabrication of the Yagi-Uda arrays is the same as previously outlined for the proximity-coupled patch antennas in Section 4.1 with two deviations:

1. Unclad Rogers LCP is used.

2. 18 layers of SU-8 are printed to achieve a dielectric thickness of 120 μm.

This process is used to realize the following multilayer stack-up: unclad 100 μm Rogers LCP, printed silver antenna topology, printed 120 μm-thick SU-8 dielectric substrate, and printed silver microstrip topology. A profilometer scan of the printed SU-8 dielectric substrate is shown in Figure 20. With the deposition of many layers, the printed substrate experiences effects from surface tension and drying thus creating as a result a convex-shaped profile [29]. Across the 300 μm X-span of the center of the substrate occupied by the microstrip feed line, a profile variation of $\pm$ 2 μm is measured, equivalent to 3% of the substrate thickness.

Images of the printed antennas are shown in Figure 21, including the 3- and 5-director antenna structures and detailed images of the printed dielectric substrate, driving dipole, and slight substrate bending upon end-launch connector mounting.

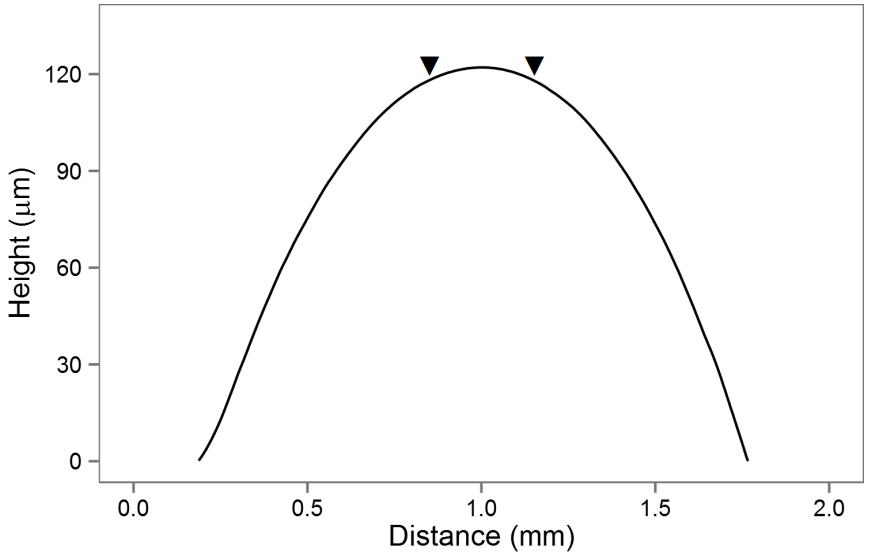

Figure 20: Profilometer scan of the printed 18-layer (120 μm thick) SU-8 dielectric substrate of the microstrip feedline, identifying the 300 μm area of the printed silver feedline (▼).

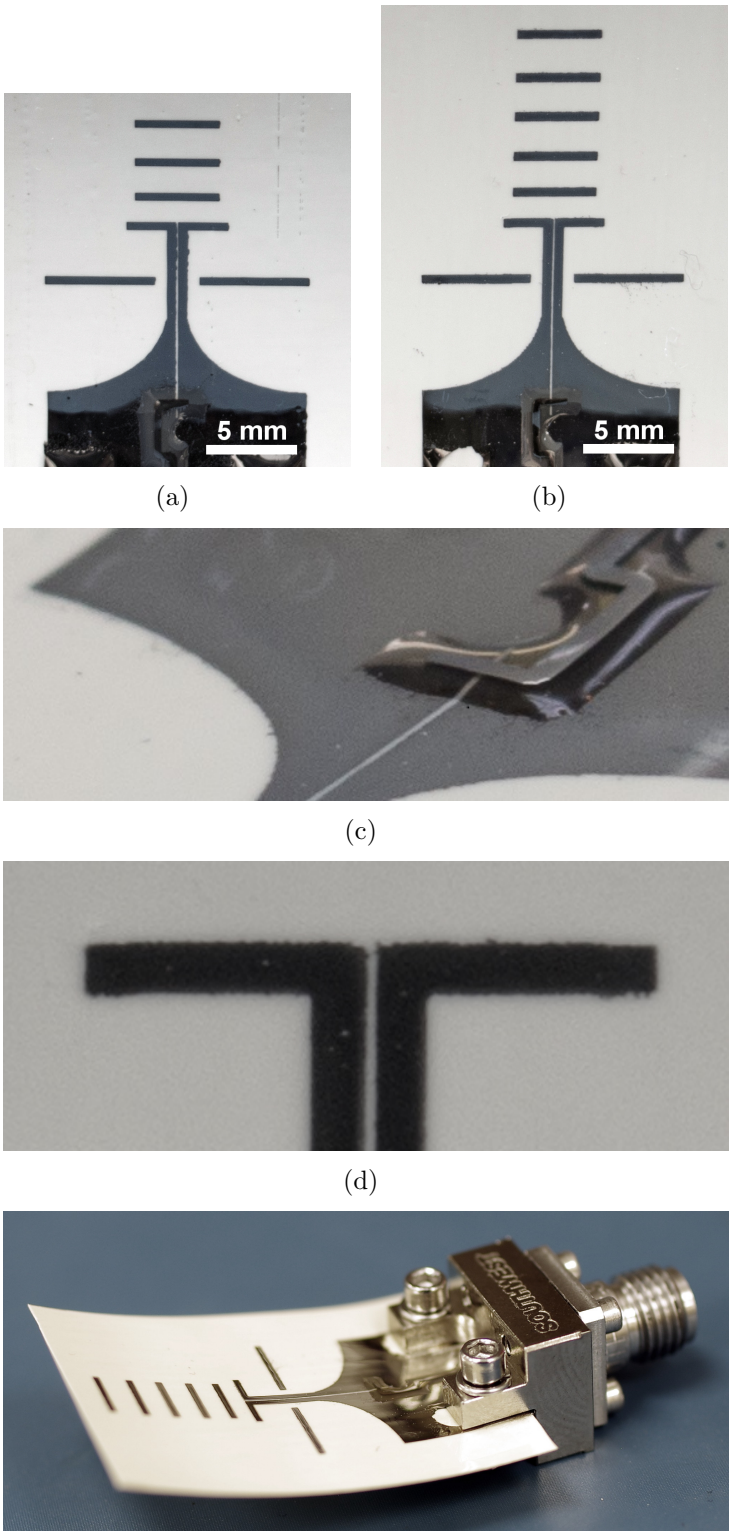

(a) (b)

(c)

(d)

(e)

Figure 21: Inkjet-printed multilayer (a) 3- and (b) 5-director Yagi-Uda antennas with detail images showing (c) the printed dielectric substrate for the microstrip-to-slotline feeding transition, (d) driving dipole, and (e) slight substrate bending.

4.2.2 Results and Analysis

Upon completion of fabrication, end-launch connectors provided by Southwest Microwave are mounted onto the antennas for RF characterization. S11 return loss measurements are then performed from 21–27 GHz using an Anritsu 37369 VNA, shown in Figure 22. Return loss measurements show good agreement with simulated results as well as efficient matching at 24.5 GHz, further demonstrating the integrity of both the metallic and dielectric ink materials used within the inkjet printing process.

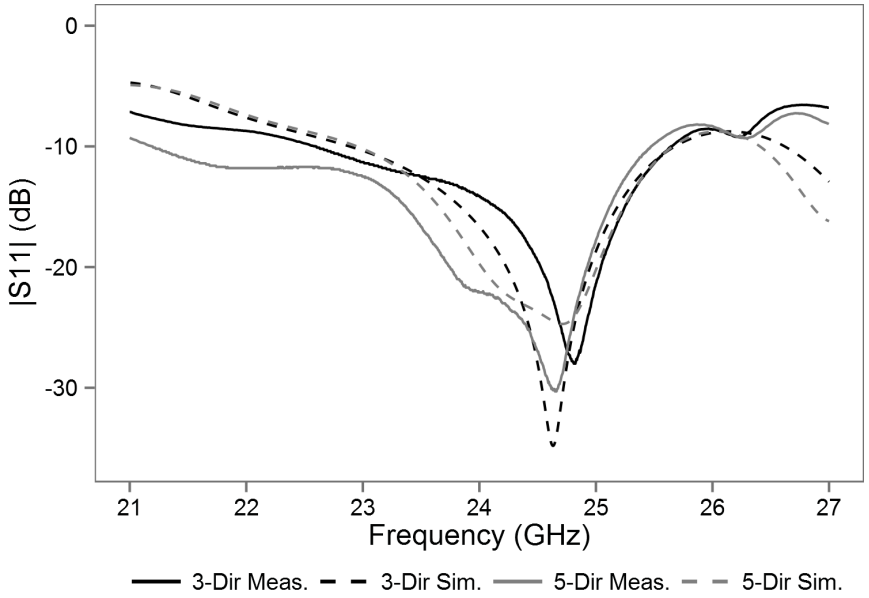

Figure 22: Simulated and measured return loss for the inkjet-printed 3 and 5-director Yagi-Uda antennas.

The realized gain of the fabricated antennas is measured with a mm-wave far-field measurement system utilizing a 20 dB standard gain horn antenna provided by Fairview Microwave (Fairview Microwave, Allen, TX, USA) at a distance of 45 cm. A plot of the measured and simulated end-fire realized gain for the 3 and 5-director antennas from 23–26 GHz is shown in Figure 23. Maximum end-fire realized gains of 6 and 8 dBi for the 3 and 5-director designs, respectively, are achieved within the 24.5 GHz ISM band. These measurements improve upon the the 7 dBi realized gain of a previous effort with a Vivaldi antenna achieved in [27], demonstrating the

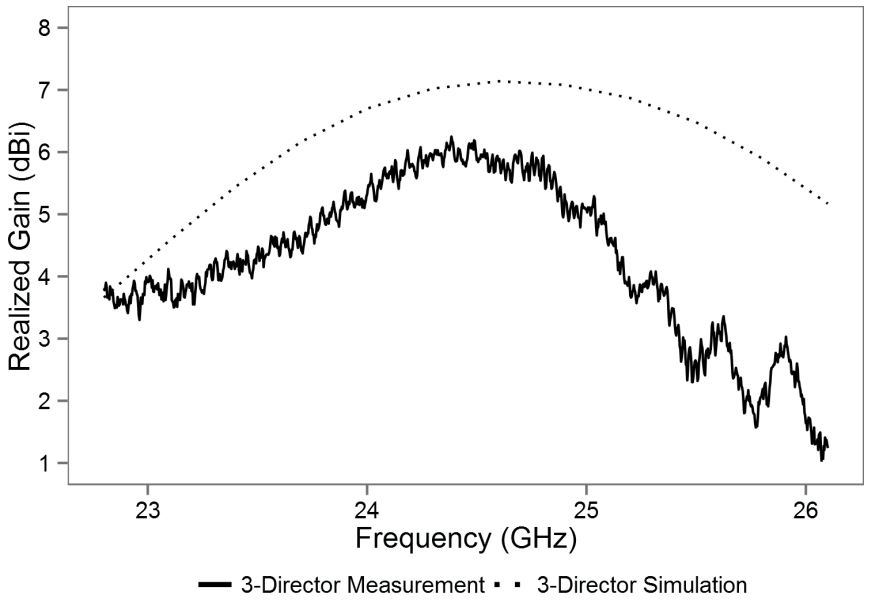

(a)

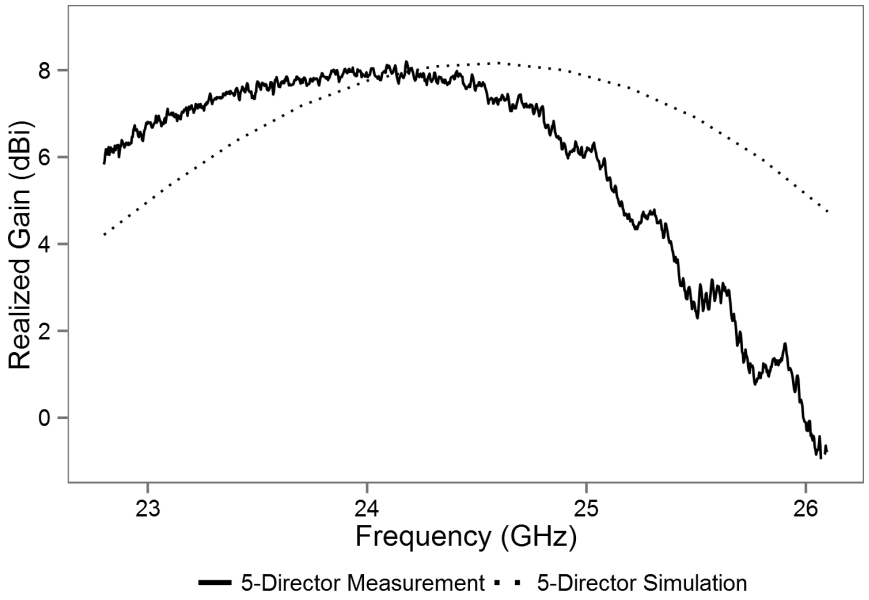

(b)

Figure 23: Simulated and measured realized gain for inkjet-printed (a) 3- and (b) 5-director Yagi-Uda antennas.

highest-gain inkjet-printed antenna within the outlined frequency band to date.

Though the measured results match well with simulated data in the lower frequencies of the measured range, discrepancies between the two in the higher frequencies are likely the result of substrate deformation during measurement as well as standing

waves present in the coaxial feed-lines of the measurement system that were unable to be removed from measurements.

The radiation patterns of the printed antennas are measured using a mm-wave far-field rotational measurement system setup with a 45 cm distance between interrogating antenna and antenna under testing. Normalized E-field radiation patterns in the X-Y (ϕ sweep) and Y-Z (θ sweep) planes of the antennas are measured and compared with simulated patterns in Figure 24. The measured Y-Z radiation pattern cuts in Figure 24(a) show excellent agreement with simulations for both the 3- and 5-director designs. The measured X-Y radiation pattern cuts in Figure 24(b) exhibit good agreement with simulations in the end-fire 0° direction but experience discrepancies with slightly enlarged side-lobes, specifically in the back-side 180° region. These deviations are likely the result of substrate bending during measurement, where a deformation in the X-Y plane of the antenna is conducive to a greater degree of error in the X-Y radiation pattern measurements. A second source of error could result from the modeling of the end-launch connector in simulations. Though the connectors were included in simulations, nonidealities present in the feeding structure model have the potential to affect the radial efficiency of the antenna in different directions.

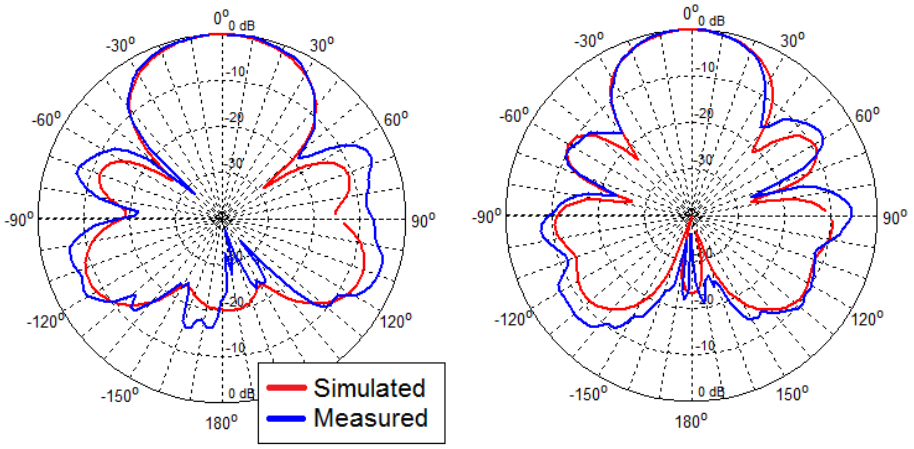

(a)

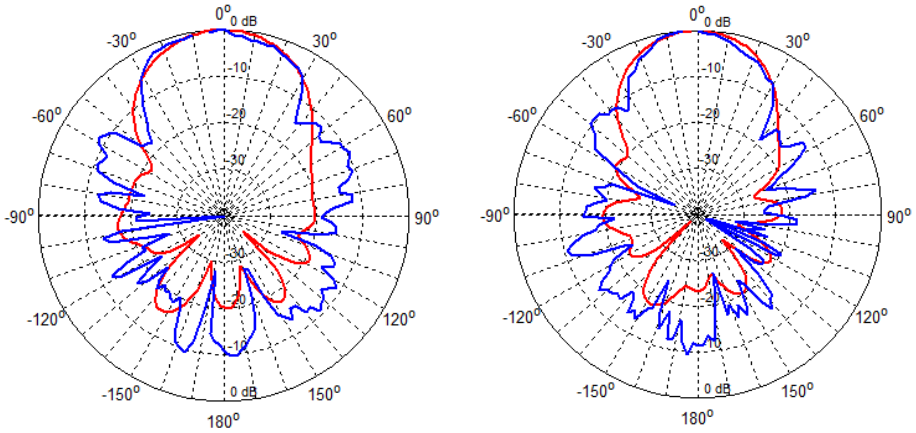

(b)

Figure 24: Simulated and measured normalized (a) Y-Z and (b) X-Y E-field radiation patterns for inkjet-printed (left) 3- and (right) 5-director Yagi-Uda antennas.

CHAPTER V

CONCLUSION

This work demonstrates the feasibility of fabricating high-gain, multilayer mm-Wave antenna structures using inkjet printing processes. Conductive and dielectric thick-film inks are characterized and presented for use with additive, vertically-integrated electronic fabrication. Several advanced processing techniques are outlined for the realization of uniform thick dielectric films to be used as selectively-patterned dielectric substrates. A proof-of-concept demonstration of this additive substrate fabrication process is presented with the first fully-printed RF structures for material characterization. Two high-gain mm-Wave antenna designs are simulated, fabricated, and measured in order to demonstrate this multilayer process, featuring multilayer dielectric stack-ups exceeding 100 μm and realized gain measurements exceeding those present in literature for inkjet-printed mm-Wave antennas.

Future advancements in this work reach throughout the electronic fabrication and packaging industries. Dielectric ink compositions can be further investigated to increase ink versatility, for example with high-K and low loss dielectrics for efficient device miniaturization. The selective patterning of thick dielectric materials has potential to be integrated with packaging schemes, such as die-level bonding and interconnects in an effort to reduce the parasitics and vertical profiles of typical wire bonding and flip-chip techniques. Frequency limits of multilayer printed antennas can be pushed into the 60 GHz ISM band for efficient integration with automotive radar and gigabit wireless communication systems. The additive nature of this process is essential to the future integration of on-chip post-processed antennas for such mm-Wave systems in a low-cost, rapid, and environmentally advantageous fashion.

REFERENCES

[1] Bisognin, A., Thielleux, J., Wei, W., Titz, D., Ferrero, F., Brachat, P., Jacquemod, G., Happy, H., and Luxey, C., "Inkjet coplanar square monopole on flexible substrate for 60-GHz applications," *Antennas and Wireless Propagation Letters, IEEE*, vol. 13, pp. 435–438, 2014.

[2] Chang, S.-H., Kuan, H., Wu, H.-W., Yang, R.-Y., and Weng, M.-H., "Determination of microwave dielectric constant by two microstrip line method combined with em simulation," *Microwave and optical technology letters*, vol. 48, no. 11, pp. 2199–2201, 2006.

[3] Chow, T., "Wetting of rough surfaces," *Journal of Physics: Condensed Matter*, vol. 10, no. 27, p. L445, 1998.

[4] Cook, B. S., *Vertical integration of inkjet-printed RF circuits and systems (VIPRE) for wireless sensing and inter/intra-chip communication applications*. PhD thesis, Georgia Institute of Technology, 2014.

[5] Cook, B., Cooper, J., and Tentzeris, M., "Multi-layer rf capacitors on flexible substrates utilizing inkjet printed dielectric polymers," *Microwave and Wireless Components Letters, IEEE*, vol. 23, pp. 353–355, July 2013.

[6] Cook, B., Mariotti, C., Cooper, J., Revier, D., Tehrani, B., Aluigi, L., Roselli, L., and Tentzeris, M., "Inkjet-printed, vertically-integrated, high-performance inductors and transformers on flexible lcp substrate," in *Microwave Symposium (IMS), 2014 IEEE MTT-S International*, pp. 1–4, June 2014.

[7] Cook, B. and Shamim, A., "Inkjet printing of novel wideband and high gain antennas on low-cost paper substrate," *Antennas and Propagation, IEEE Transactions on*, vol. 60, pp. 4148–4156, Sept 2012.

[8] Cook, B., Tehrani, B., Cooper, J., and Tentzeris, M., "Multilayer inkjet printing of millimeter-wave proximity-fed patch arrays on flexible substrates," *Antennas and Wireless Propagation Letters, IEEE*, vol. 12, pp. 1351–1354, 2013.

[9] Falat, T., Felba, J., Moscicki, A., and Borecki, J., "Nano-silver inkjet printed interconnections through the microvias for flexible electronics," in *Nanotechnology (IEEE-NANO), 2011 11th IEEE Conference on*, pp. 473–477, IEEE, 2011.

[10] Ghannam, A., Viallon, C., Bourrier, D., and Parra, T., "Dielectric microwave characterization of the su-8 thick resin used in an above ic process,"

in *Microwave Conference, 2009. EuMC 2009. European*, pp. 1041–1044, IEEE, 2009.

[11] Hage-Ali, S., Tiercelin, N., Coquet, P., Sauleau, R., Fujita, H., Preobrazhensky, V., and Pernod, P., "A millimeter-wave microstrip antenna array on ultra-flexible micromachined polydimethylsiloxane (pdms) polymer," *Antennas and Wireless Propagation Letters, IEEE*, vol. 8, pp. 1306–1309, 2009.

[12] Hettak, K., Ross, T., James, R., Momciu, A., and Wight, J., "Flexible polyethylene terephthalate-based inkjet printed CPW-fed monopole antenna for 60 GHz ISM applications," in *Microwave Conference (EuMC), 2013 European*, pp. 1447–1450, Oct 2013.

[13] Kawase, T., Sirringhaus, H., Friend, R. H., and Shimoda, T., "Inkjet printed via-hole interconnections and resistors for all-polymer transistor circuits," *Advanced Materials*, vol. 13, no. 21, p. 1601, 2001.

[14] Keller, S., Blagoi, G., Lillemose, M., Haefliger, D., and Boisen, A., "Processing of thin su-8 films," *Journal of Micromechanics and Microengineering*, vol. 18, no. 12, p. 125020, 2008.

[15] Kim, S., *Inkjet-printed Sensors and Via-enabled Structures for Low-cost Autonomous Wireless Platforms*. PhD thesis, Georgia Institute of Technology, 2014.

[16] Ko, S. H., Chung, J., Pan, H., Grigoropoulos, C. P., and Poulikakos, D., "Fabrication of multilayer passive and active electric components on polymer using inkjet printing and low temperature laser processing," *Sensors and Actuators A: Physical*, vol. 134, no. 1, pp. 161 – 168, 2007.

[17] Kumar, K. and Gunasekaran, N., "A novel wideband slotted mm wave microstrip patch antenna," in *International Conference on Signal Processing, Communication, Computing and Networking Technologies (ICSCCN)*, pp. 10–14, July 2011.

[18] Latti, K.-P., Kettunen, M., Strom, J.-P., and Silventoinen, P., "A review of microstrip t-resonator method in determining the dielectric properties of printed circuit board materials," *Instrumentation and Measurement, IEEE Transactions on*, vol. 56, no. 5, pp. 1845–1850, 2007.

[19] Li, J., Ye, F., Vaziri, S., Muhammed, M., Lemme, M. C., and stling, M., "Efficient inkjet printing of graphene," *Advanced Materials*, vol. 25, no. 29, pp. 3985–3992, 2013.

[20] ling Kao, H., Yeh, C.-S., Zhang, X. Y., Cho, C.-L., Dai, X., Wei, B.-H., Chang, L.-C., and Chiu, H.-C., "Inkjet printed series-fed two-dipole antenna comprising a balun filter on liquid crystal polymer substrate," *Components, Packaging and Manufacturing Technology, IEEE Transactions on*, vol. 4, pp. 1228–1236, July 2014.

[21] Maza, A., Cook, B., Jabbour, G., and Shamim, A., "Paper-based inkjet-printed ultra-wideband fractal antennas," *Microwaves, Antennas Propagation, IET*, vol. 6, pp. 1366–1373, September 2012.

[22] Reinhold, I., Thielen, M., Voit, W., Zapka, W., Gotzen, R., and Bohlmann, H., "Inkjet printing of electrical vias," in *Microelectronics and Packaging Conference (EMPC), 2011 18th European*, pp. 1–4, IEEE, 2011.

[23] Seok, S., Rolland, N., and Rolland, P.-A., "Millimeter-wave quarter-wave patch antenna on benzocyclobutene polymer," in *Microwave Conference, 2008. EuMC 2008. 38th European*, pp. 1018–1021, Oct 2008.

[24] Shuppert, B., "Microstrip/slotline transitions: modeling and experimental investigation," *Microwave Theory and Techniques, IEEE Transactions on*, vol. 36, pp. 1272–1282, Aug 1988.

[25] Spider Graphics, *DIMATIX Printer Tutorial and Operating Instructions*, 2014.

[26] Subramanian, V., Chang, P., Lee, J., Molesa, S., and Volkman, S., "Printed organic transistors for ultra-low-cost rfid applications," *Components and Packaging Technologies, IEEE Transactions on*, vol. 28, pp. 742–747, Dec 2005.

[27] Tehrani, B., Cook, B., Cooper, J., and Tentzeris, M., "Inkjet printing of a wideband, high gain mm-wave Vivaldi antenna on a flexible organic substrate," in *Antennas and Propagation Society International Symposium (APS/URSI), 2014 IEEE*, pp. 320–321, July 2014.

[28] Tehrani, B., Cook, B., and Tentzeris, M., "Post-process fabrication of multilayer mm-wave on-package antennas with inkjet printing," in *Antennas and Propagation Society International Symposium (APS/URSI), 2015 IEEE*, July 2015.

[29] Tehrani, B., Bito, J., Cook, B., and Tentzeris, M., "Fully inkjet-printed multilayer microstrip and t-resonator structures for the RF characterization of printable materials and interconnects," in *Microwave Symposium (IMS), 2014 IEEE MTT-S International*, pp. 1–4, June 2014.

[30] Tehrani, B., Cook, B., and Tentzeris, M., "Inkjet printing of multilayer millimeter-wave yagi-uda antennas on flexible substrates," *Antennas and Wireless Propagation Letters, IEEE*, 2015. Under Review.

[31] Yang, L., Rida, A., Vyas, R., and Tentzeris, M., "Rfid tag and rf structures on a paper substrate using inkjet-printing technology," *Microwave Theory and Techniques, IEEE Transactions on*, vol. 55, pp. 2894–2901, Dec 2007.

[32] Zou, G., Gronqvist, H., Starski, J. P., and Liu, J., "Characterization of liquid crystal polymer for high frequency system-in-a-package applications," *Advanced Packaging, IEEE Transactions on*, vol. 25, no. 4, pp. 503–508, 2002.